Decentralized Bidirectional Voltage Supporting Control for Multi-Mode Hybrid AC/DC Microgrid

Yang, Pengcheng; Yu, Miao; Wu, Qiuwei; Hatziargyriou, Nikos; Xia, Yanghong; Wei, Wei

Published in:
IEEE Transactions on Smart Grid

Link to article, DOI:
10.1109/tsg.2019.2958868

Publication date:
2020

Document Version
Peer reviewed version

Decentralized Bidirectional Voltage Supporting Control for Multi-Mode Hybrid AC/DC Microgrid

Pengcheng Yang, *Student Member, IEEE,* Miao Yu, *Member, IEEE,* Qiuwei Wu, *Senior Member, IEEE,* Nikos Hatziargyriou, *Fellow, IEEE,* Yanghong Xia, *Student Member, IEEE and* Wei Wei

***Abstract*— A hybrid ac/dc microgrid consists of alternating current (ac) subgrid(s), direct current (dc) subgrid(s) and intermediate bidirectional power converters (BPCs). The presence of dc distribution networks complicates the operation and corresponding control of the hybrid ac/dc microgrid. This paper proposes a decentralized bidirectional voltage supporting control scheme for the multi-mode hybrid ac/dc microgrid, which can provide uninterruptable ac and dc voltages in case of unintentional ac and dc islanding events. An ac phase angle – dc voltage inverse droop control with virtual impedance are designed and implemented in BPCs, which can support the ac and dc voltages and enable seamless mode switching without additional voltage sources. Proper power sharing between ac and dc subgrids is realized without frequency deviation in the ac islanded mode. The stability of proposed control is analyzed under different modes, and its performance is verified by real-time hardware-in-loop (HIL) tests.**

***Index Terms*-- Bidirectional power converter, bidirectional voltage support, inverse droop control, multi-mode hybrid ac/dc microgrid, seamless mode switching.**

I. Introduction

THE concept of microgrid has been proposed as an efficient solution for reliable integration of distributed generators (DGs), energy storage and controllable loads [1], [2]. Recently, with the increasing penetration of direct current (dc) DGs and dc loads such as photovoltaic (PV) units, batteries, electric vehicles (EVs), LED lights, etc., the traditional microgrid includes numerous alternating current (ac)/dc conversions[3]. To effectively integrate various types of ac/dc DGs and loads with reduced conversion stages, the hybrid ac/dc microgrid is proposed, which consists of the ac subgrid with ac DG and ac loads and the dc subgrid with dc DGs and dc loads, as shown in Fig.1 [4]-[6]. The bidirectional power converters (BPCs) connect and coordinate the ac and dc subgrids.

For the traditional ac microgrid, there are two operation modes, grid-connected mode and islanded mode, which are determined by the connection status with the ac distribution network. With the emergence of modular cascaded converters (MCCs) technology and the resulting MCC based dc transformer, the dc distribution network can provide higher efficiency, power density, flexibility compared to the ac distribution network [7], [8]. Coupling the dc distribution network with the dc subgrid of the hybrid ac/dc microgrid, can provide robust voltage support for the dc subgrid and efficient dc load sharing through the dc transformer [9]. The connection of the hybrid ac/dc microgrid with both ac and dc distribution networks however makes its operation more complicated than tradition ac microgrid.

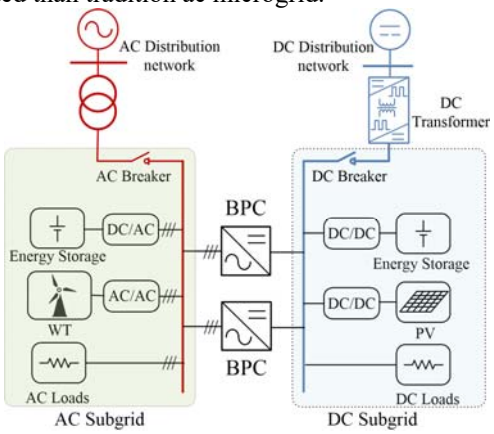

Fig. 1. Topology of hybrid ac/dc microgrid in this paper

When the traditional microgrid operates in grid-connected mode, the voltage can be supported by the distribution network, while in islanded mode, voltage support is provided by a voltage source. During the switching process from interconnected to islanded mode, the detection of an islanding event is imperative for the voltage sources. The available islanding detection algorithms, both passive and active methods need to compromise between speed and accuracy, while further research is needed to accommodate low-inertia systems [10]-[13]. Alternative to the islanding detection, the droop control, which was firstly applied on the uninterruptible power supply (UPS) systems, has been extended to the voltage support of a microgrid [14]. By setting the frequency and voltage magnitude deviations proportional to the active and reactive output power, the droop control can coordinate multiple voltage sources and the distribution grid, and realize voltage support and power sharing in both grid-connected and islanded modes [15], [16]. This provides seamless mode switching without islanding detection [17].

However, conventional droop suffers from well-known limitations, such as inherent frequency and voltage magnitude deviations, sensitivity of sharing accuracy to line impedance [18], [19], and economic inefficiency. In practice, the dispatchable DGs like micro turbines, diesel generators, fuel cells and energy storages (ESs) usually serve as voltage sources. Comparing with

This work is supported in part by the National Key R&D Program of China(2018YFB0904700)

P. Yang, M. Yu, Y. Xia and W. Wei are with the Zhejiang University, Hangzhou, 310027, China. (e-mail: ypc196@zju.edu.cn, zjuyumiao@zju.edu.cn, royxiayh@126.com, wwei@zju.edu.cn)

Q. Wu is with the Centre for Electric Power and Energy, Department of Electrical Engineering, Technical University of Denmark, Lyngby, 2800, Denmark. (e-mail: qw@elektro.dtu.dk).

N. Hatziargyriou is with the School of Electrical and Computer Engineering, National Technical University of Athens, 15780 Athens, Greece (e-mail: nh@power.ece.ntua.gr)

renewable undispatchable DGs, such as PV units and wind turbines (WTs), the generation cost of voltage sources is much higher because of the fuel cost or lifecycle cost of the ES [20]-[22]. To ensure uninterrupted voltage in case of an unintentional grid fault, the droop controlled voltage sources need to operate as backup power during the grid-connected mode. Consequently, the full-time operation of these voltage sources in both grid-connected mode and islanded mode makes microgrid operation costly.

For the conventional hybrid ac/dc microgrid, in case of a fault on the ac or dc distribution grid, both ac and dc subgrids need voltage sources. Hence, there are at least two dispatchable DGs or ESs serving as voltage sources in the hybrid ac/dc microgrid. This is not necessary if BPCs are used to support the voltage [23], [24]. In [23], only one voltage source is required in the ac subgrid. The voltage of the dc subgrid is maintained by BPCs. In [24], the sole voltage source is used to support voltage of the dc subgrid. For the ac subgrid, the modified ac frequency and magnitude droop control are employed on BPCs to support ac voltage. The number of voltage sources is reduced to one with the BPCs supporting one subgrid. Furthermore, if the BPCs can support the voltages of both subgrids bidirectionally, the use of voltage sources is not required under certain fault conditions.

In [25] and [26], the unified BPC control is firstly proposed to support voltages of both ac and dc subgrids. By feeding back the measured ac frequency and dc voltage, the unified control regulates the power reference [25] and frequency reference [26] of the power-frequency ($P-f$) droop control, which essentially changes the power exchange between the two subgrids to maintain the voltage balance of the two subgrids. With the unified BPC control, the BPCs can flexibly support the subgrid without a voltage source. However, the $P-f$ droop based unified control results in frequency deviations in the ac subgrid. Besides, the voltage sources still need to operate full-time to provide uninterrupted voltage in case of unintentional islanding.

In this paper, a decentralized bidirectional voltage supporting control is proposed for the multi-mode hybrid ac/dc microgrid, which can provide uninterruptable ac and dc voltage support without control method switching or full-time operation of voltage sources. The main features of the proposed control are summarized as follows:

1) The operation of the hybrid ac/dc microgrid coupled with ac and dc distribution networks is analyzed and classified into four modes. Four switch principles are proposed for flexible mode switching in order to minimize the power fluctuations during transition and prolong the lifetime of the ESs.

2) A compact ac phase angle – dc voltage ($\theta - v_{dc}$) inverse droop control is designed for BPCs, which can help supporting the ac and dc voltages bidirectionally without frequency deviation, in case of unintentional ac and dc islanding events. The proposed bidirectional support enables the seamless transfer with minimal dependence on additional voltage sources.

3) By adopting the designed virtual impedance and $\theta - v_{dc}$ inverse droop coefficient, the power can be proportionally shared among multiple BPCs according to BPCs' capacities. Furthermore, when there is a power fluctuation in one subgrid, the other subgrid can coordinately share the fluctuation according to subgrids' capacities, thus reducing the pressure on one single subgrid.

The rest of this paper is organized as follows. In Section II, the operation modes and mode switching principles of the hybrid ac/dc microgrid are introduced. In Section III, bidirectional voltage support control for the multi-mode hybrid ac/dc microgrid is proposed. In Section IV, the small signal model of the hybrid microgrid is established to analyze the stability in different modes. In Section V, the HIL test results are presented to verify the efficiency of the proposed control, followed by the conclusions.

II. Operation Modes of Hybrid AC/DC Microgrid

A. Classification of Operation Modes

For the traditional ac or dc microgrid, there are two operation modes, grid-connected mode and islanded mode, which are characterized by the connection status with the upstream distribution network. For the hybrid ac/dc microgrid of Fig.1, there are four operation modes according to the connection with the ac and dc upstream distribution network:

1) Mode I: Both ac and dc subgrids are grid-connected (AC/DC-GC mode), the ac and dc breakers are closed.
2) Mode II: The ac subgrid is grid-connected and dc subgrid islanded (AC-GC DC-IS). The ac breaker is closed, the dc breaker is open.
3) Mode III: Both ac and dc subgrids are islanded (AC/DC-IS mode), the ac and dc breakers are open.
4) Mode IV: The ac subgrid is islanded and dc subgrid grid-connected (AC-IS DC-GC mode), the ac breaker is open, the dc breaker is closed.

In Mode I, the voltage of ac and dc bus can be supported by ac and dc units, and the load can be balanced by ac and dc units. In Mode II, a dc voltage source is needed to form the dc subgrid voltage, and the power balance can only be maintained by ac units and ESs. In Mode III, both ac and dc voltage sources are required to support the voltage of ac and dc subgrids. In Mode IV, an ac voltage source is needed for ac voltage support.

B. Mode switching Principles for Hybrid ac/dc Microgrid

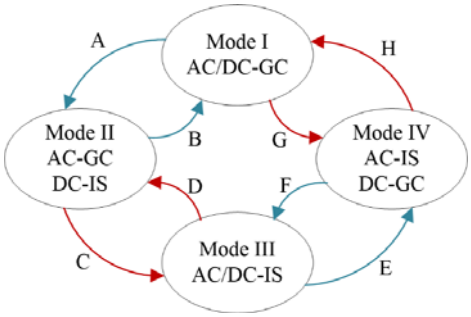

Fig. 2. The eight Mode switching paths between four modes.

The hybrid ac/dc microgrid usually operates in the AC/DC-GC mode. When there is a fault on the ac or dc upstream distribution grid, the corresponding ac or dc breaker will open to isolate the fault. The breakers will reclose to connect with grids after the synchronization till the fault is cleared. The operation mode of the hybrid microgrid will change when the breakers operate. The mode switching paths among the four modes are shown in Fig. 2. There are eight switching paths labeled by A to H.

To realize the switching between two modes, there are always many path options. For example, both path sequences A→C and G→F realize the switching from Mode I to Mode III. To get the best optional sequence, the transferred power is introduced to evaluate the different path sequences. For the paths A, B, E, F, the transferred power is $\left|P_{dc,pcc}\right|$, which is the absolute value of

TABLE I
Mode Switching Paths between four modes

The initial mode / The next mode	I	II	III	IV
I	\	B	If $\lvert P_{ac,pcc}\rvert \geq \lvert P_{dc,pcc}\rvert$, E→H If $\lvert P_{ac,pcc}\rvert < \lvert P_{dc,pcc}\rvert$, D→B	H
II	A	\	D	H→A
III	If $\lvert P_{ac,pcc}\rvert \geq \lvert P_{dc,pcc}\rvert$, A→C If $\lvert P_{ac,pcc}\rvert < \lvert P_{dc,pcc}\rvert$, G→F	C	\	F
IV	G	B→G	E	\

changed power when the dc breaker operates, and for the paths C, D, H, G, the transferred power is $\left|P_{ac,pcc}\right|$, which is the absolute value of changed power when the ac breaker operates. To minimize the power fluctuation of the mode switching process and prolong the life time of the ESs, four principles for the mode switching are proposed

1) Only one breaker can switch at a time;
2) The breaker switch times of the path sequence should be minimal;
3) If two breakers need to open, the breaker with lower transferred power switches first; if two breakers need to close, the breaker with higher transferred power switches first;
4) If one breaker needs to open, and the other breaker needs to close, the switch-on breaker switches first.

Principle (1) ensures that ac and dc breakers cannot operate simultaneously, which can cause severe power fluctuations in both ac and dc side. Principle (2) is the switching principle between the adjacent modes like Mode I and Mode II, there are two switching path sequences from Mode I to Mode II: 1) A; 2) G→F→D. The transferred power of path A is $\left|P_{dc,pcc}\right|$, and the transferred power of G→F→D is $\left|P_{dc,pcc}\right| + 2\left|P_{ac,pcc}\right|$, which indicates that there is more power change than in path A. Principles (3) and (4) are proposed to conduct the switching between the nonadjacent modes. For nonadjacent mode switching, like from Mode I to Mode III, the transferred power of sequences A→C and G→F is equal to $\left|P_{ac,pcc}\right| + \left|P_{dc,pcc}\right|$. To choose a better switching sequence, we need to compare the transition mode of the two path sequences. For path sequence A→C, the transition mode is Mode II. The hybrid microgrid is supported by the ac distribution network and the ESs in Mode II, and the power fluctuation is also shared by the ac distribution network and the ESs. The transferred power $\left|P_{ac,pcc}\right|$ can quantify the support by the ac distribution network. With higher $\left|P_{ac,pcc}\right|$, the ac distribution network will share more power fluctuation, which can release the pressure of the ESs and prolong its life time. For the path sequence G→F, the transition mode is Mode IV. The hybrid microgrid is supported by the dc distribution network and the ESs in Mode IV. Similarly, the more power is shared by the dc distribution network, the less pressure will be exerted on the ESs. In this way, Principle (3) solves the switching between Mode I and Mode III, the path sequence with higher transferred power transition mode is preferred to prolong the ESs's life time. Principle (4) deals with the switching between Mode II and Mode IV, the transition modes are Mode I and Mode III. Obviously, with the support by ac and dc distribution networks, the ESs in Mode I shares less power fluctuations than in Mode III. Hence, Mode I is selected as the transition mode, and the switching path sequence can only be B→G or H→A between Mode II and Mode IV. According to the principles (1)–(4), the mode switching process can minimize the power fluctuations during switching and prolong the life time of the ESs. Detailed switching paths between the four modes are illustrated in Table I.

III. Bidirectional Voltage Supporting Control

In this section, the bidirectional voltage control for the BPCs in the hybrid ac/dc microgrid, is proposed. This control mode can form ac and dc voltages whenever there is an unintentional islanding event in the ac side or dc side, respectively. Firstly, a virtual impedance is designed in the ac side of the BPC. Based on the virtual impedance, the rated frequency and ac voltage magnitude control is adopted to support ac voltage and share the ac load. Secondly, an ac phase angle-dc voltage inverse droop control is designed to support the dc voltage and share dc load. Finally, a bidirectional supporting controller is designed for BPCs with the mode switching in Section II.

A. Ac Voltage Control

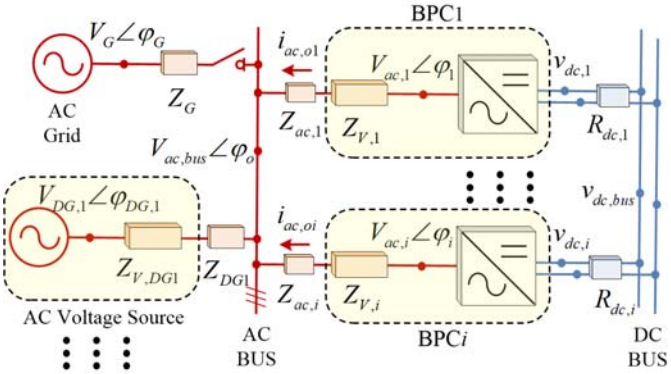

Fig. 3. Topology of ac subgrid.

When there is an unintentional islanding event on the ac side, the ac grid voltage is unavailable, and the BPCs need to form the ac voltage for the ac subgrid. The voltage magnitude, frequency and phase angle are main issues of ac voltage control. In this paper, the rated magnitude V^* and rated frequency f^* are used for BPCs, and the ac phase angle-dc voltage $\theta - v_{dc}$ inverse droop is used to determine the ac phase angle θ_i. The reference output ac voltage $v_{ac,i}^{ref}$ of BPC$_i$ is obtained as

$$v_{ac,i}^{ref} = V^* \sin(\varphi_i) = V^* \sin(2\pi f^* \cdot t + \theta_i). \quad (1)$$

By adopting the direct voltage control with rated magnitude, rated frequency and adjustable phase angle in (1), the ac voltage can be supported by BPCs, and there is no frequency deviation in the ac islanded mode. However the proper power sharing between BPCs will be quite difficult. In high-voltage ac distribution

networks, the line impedance is inductive. By adjusting the phase angle and magnitude, the decoupled active power (P) and reactive power (Q) can be regulated, respectively. However, in low-voltage ac subgrids, the P-Q coupling is problematic due to the nontrivial line resistance. This problem is resolved by adopting a virtual impedance to shape the output impedance of BPCs and ac voltage sources, as shown in Fig. 3. The virtual impedance Z_v of BPC is designed as pure inductance X_v and is much larger than the actual line impedance $Z_{ac,i}$. The power output of BPC_i can be expressed as

$$P_{ac,BPCi} = \frac{3V^*V_{ac,bus}}{2X_{v,i}}\sin(\varphi_i - \varphi_o) \approx \frac{3V^*V_{ac,bus}}{2X_{v,i}}(\theta_i - \theta_o), \quad (2)$$

$$Q_{ac,BPCi} = \frac{3V^*V_{ac,bus}\cdot\cos(\varphi_i-\varphi_o)-V_{ac,bus}^2}{2X_{v,i}} \approx \frac{3(V^*-V_{ac,bus})\cdot V_{ac,bus}}{2X_{v,i}}, \quad (3)$$

where $V_{ac,bus}$ and $\varphi_o = 2\pi f^* \cdot t + \theta_o$ are the magnitude and phase angle of the ac bus voltage, and the phase angle difference $\varphi_i - \varphi_o$ is small. In the $\theta - v_{dc}$ inverse droop, θ_i is determined by the dc voltage drop of BPC_i, and θ_i can be considered as the same for all BPCs, as detailed in the next subsection.

From (2) and (3), the power injected into ac bus is proportional to the reciprocal of BPC's virtual impedance. In this way, by considering the BPCs' capacity in the virtual impedance design, the power sharing can be set as proportional to the BPCs' capacity, as

$$P_{ac,BPC1}:P_{ac,BPC2}:\cdots:P_{ac,BPCi} = X_{v,1}^{-1}:X_{v,2}^{-1}:\cdots:X_{v,i}^{-1} = C_{BPC1}:C_{BPC2}:\cdots:C_{BPCi}, \quad (4)$$

$$Q_{ac,BPC1}:Q_{ac,BPC2}:\cdots:Q_{ac,BPCi} = X_{v,1}^{-1}:X_{v,2}^{-1}:\cdots:X_{v,i}^{-1} = C_{BPC1}:C_{BPC2}:\cdots:C_{BPCi}, \quad (5)$$

where C_{BPCi} is the capacity of BPC_i.

By adopting the control strategy in (1) and designed virtual impedance ratio in (4), the ac voltage can be supported by the BPCs in the AC-IS mode, and the power sharing between BPCs is proportional to their capacities. |

While in the AC-GC mode, the power is shared not only between BPCs, but also with the ac grid. This is more complicated than the AC-IS mode. The virtual impedance of BPC is further designed to facilitate the power sharing in the AC-GC mode.

The ac grid is usually represented by a rated voltage source $V^*\sin(2\pi f^* \cdot t)$ and inductive impedance Z_G with inductance X_G. The power output of ac grid is

$$P_{ac,pcc} = \frac{3V^*\cdot V_{ac,bus}}{2X_G}\sin(\varphi_G - \varphi_o) \approx \frac{3V^*\cdot V_{ac,bus}}{2X_G}(-\theta_o), \quad (6)$$

$$Q_{ac,pcc} = \frac{3V^*V_{ac,bus}\cdot\cos(\varphi_G-\varphi_o)-V_{ac,bus}^2}{2X_G} \approx \frac{3(V^*-V_{ac,bus})\cdot V_{ac,bus}}{2X_G}, \quad (7)$$

where $\varphi_G = 2\pi f^* \cdot t$ is the phase angle of the upstream network.

If there are ac voltage sources in the ac subgrid in Fig. 3, the power should also be shared by ac voltage sources. Setting the rated magnitude V^* and rated frequency f^* for the ac voltage sources, their power output can be expressed as,

$$P_{ac,DGj} = \frac{3}{2}\cdot\frac{V^*V_{ac,bus}}{X_{DG,j}}(-\theta_o), \quad (8)$$

$$Q_{ac,DGj} = \frac{3}{2}\cdot\frac{(V^*-V_{ac,bus})\cdot V_{ac,bus}}{X_{DG,j}}, \quad (9)$$

where $X_{DG,j}$ is the inductance of the virtual impedance $Z_{DG,j}$ of ac voltage source DG_j.

With a load fluctuation $\Delta P_{ac,load}$ in the ac load, the ac bus phase angle will reflect this fluctuation with a variation of $\Delta\theta_o$. The ac grid, BPCs and ac voltage sources share a common θ_o according to (2), (6) and (8). Consequently, their power output will respond simultaneous to share the fluctuation. The fluctuation sharing radio is proportional to the reciprocal of their impedance according to (2), (6) and (8).

$$\Delta P_{ac,pcc}:\Delta P_{ac,DG1}:\cdots\Delta P_{ac,DGj}:\Delta P_{ac,BPC1}:\cdots:\Delta P_{ac,BPCi}:\cdots = X_G^{-1}:X_{DG,1}^{-1}:\cdots:X_{DG,j}^{-1}:X_{v,1}^{-1}:\cdots:X_{v,i}^{-1}, \quad (10)$$

where $\Delta P_{ac,pcc}$, $\Delta P_{ac,DGj}$ and $\Delta P_{ac,BPCi}$ are the power fluctuations of the ac grid, ac voltage source DG_j and BPC_i, respectively. Besides, these power fluctuations respect the constraint of power balance,

$$\Delta P_{ac,load} = \Delta P_{ac,pcc} + \sum_{j=1}^{N}\Delta P_{ac,DGj} + \sum_{i=1}^{M}\Delta P_{ac,BPCi}, \quad (11)$$

where N is the number of ac voltage sources, and M is the number of BPCs.

When sharing the ac subgrid's power fluctuation, the dc subgrid can be viewed as an ac voltage source. The power of BPCs comes from the dc subgrid. Hence, the sum of power sharing of BPCs should be proportional to the dc subgrid's capacity, which can be expressed as

$$\frac{\Delta P_{ac,pcc}+\sum_{j=1}^{N}\Delta P_{ac,DGj}}{\sum_{i=1}^{M}\Delta P_{ac,BPCi}} = \frac{C_{AC}}{C_{DC}}, \quad (12)$$

where C_{AC} and C_{DC} are capacities of the ac subgrid and dc subgrid, respectively.

By combining (4), (10) and (12), the virtual impedance of BPC_i can be obtained as

$$X_{v,i}^{-1} = X_{AC}^{-1}\cdot\frac{C_{BPCi}}{C_{BPCsum}}\cdot\frac{C_{DC}}{C_{AC}}, \quad (13)$$

where X_{AC} is viewed as equivalent impedance of the ac subgrid, and $X_{AC}^{-1} = X_G^{-1} + \sum_{j=1}^{N}X_{DGj}^{-1}$.

With the designed virtual impedance in (13), the ac load fluctuation can be properly shared by both ac and dc subgrids via BPCs in the AC-GC mode. The sharing radio is proportional to subgrids' capacities. As such, the proposed control strategy can achieve proper power sharing in both AC-GC and AC-IS modes, and support the ac voltage when there is an ac unintentional islanding.

B. Dc Voltage Supporting Control

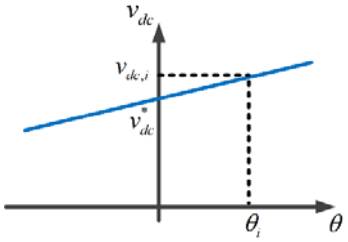

Fig. 4. The $\theta - v_{dc}$ inverse droop control.

When there is unintentional islanding event of the dc subgrid and there are no other dc voltage sources, the dc voltage must be supported by the BPCs. In this situation, the ac subgrid can be viewed as a dc voltage source. Ignoring the power loss on the BPC_i, the power injected from the ac subgrid into the dc subgrid is

$$P_{dc,BPCi} = -P_{ac,BPCi} = -\frac{3}{2}\cdot\frac{V^*V_{ac,bus}}{X_{v,i}}\theta_i + \frac{3}{2}\cdot\frac{V^*V_{ac,bus}}{X_{v,i}}\theta_o, \quad (14)$$

where $V_{ac,bus}$ and θ_o is the magnitude and phase angle of the ac subgrid bus voltage, which are considered as constant during the dynamics of the dc side. $V_{ac,bus}$ can be replaced by the rated ac magnitude V^* within an acceptable deviation. From (14), by adjusting θ_i, the power injected into the dc subgrid can be changed to supply the dc demand, and support the dc voltage. By introducing the dc voltage feedback to the ac phase angle control, the $\theta - v_{dc}$ inverse droop is designed to regulate the ac voltage phase angle as,

$$\theta_i = -m(v_{dc}^* - v_{dc,i}), \quad (15)$$

where m is the coefficient of $\theta - v_{dc}$ inverse droop control. By adopting the $\theta - v_{dc}$ inverse droop control, the dc voltage is fed

back to the phase angle, which can directly determine the power injected into the dc subgrid according to (14). The dynamic changes are fast enough to form the dc voltage, whenever the dc voltage of the upstream grid is lost. Therefore, the hybrid microgrid can seamlessly switch into the DG-IS mode during a dc unintentional islanding.

In the DC-GC mode, the dc voltage can be supported by BPCs, dc grid and other dc voltage sources. In this mode, power sharing among them is the main issue. For BPCs, substituting (15) to (14), we have

$$P_{dc,BPCi} = \frac{3}{2} \cdot \frac{V^{*2} \cdot m}{X_{v,i}} (v_{dc}^* - v_{dc,i}) + P_{dc,BPCi}^*, \quad (16)$$

where $P_{dc,BPCi}^*$ is $3V^{*2} \cdot \theta_o / 2X_{v,i}$ is considered as constant. From (16), the dc power output of BPC_i is proportional to the dc voltage deviation. For the power output of dc grid $P_{dc,pcc}$ and dc voltage sources $P_{dc,DGj}$, the $P - v_{dc}$ droop is usually adopted for the dc transformer and dc voltage source converters, and their power output is also proportional to their dc voltage deviation,

$$P_{dc,pcc} = m_G (v_{dc}^* - v_{dc,G}), \quad (17)$$

$$P_{dc,DGj} = m_{DG,j} (v_{dc}^* - v_{dc,DGj}), \quad (18)$$

where m_G and $m_{DG,j}$ are the droop coefficients of dc transformer and dc voltage source DG_j, $v_{dc,G}$ and $v_{dc,DGj}$ are the output voltage of dc transformer and dc voltage source DG_j.

Compared with the voltage deviation caused by droop control, the voltage drop caused by the dc line impedance is negligible [27]. In this way, $v_{dc,i}$, $v_{dc,pcc}$ and $v_{dc,DGj}$ can be viewed as equal to the dc bus voltage $v_{dc,bus}$. Considering load fluctuation $\Delta P_{dc,load}$ in the dc subgrid, the dc bus voltage will change by $\Delta v_{dc,bus}$ correspondingly. The dc grid, BPCs and dc voltage sources share a common $v_{dc,bus}$ according to (16), (17) and (18). Therefore, their output P will change concurrently to share the power. The power fluctuation sharing radio is

$$\Delta P_{dc,pcc} : \Delta P_{dc,DG1} : \cdots : \Delta P_{dc,DGj} : \Delta P_{dc,BPC1} : \cdots : \Delta P_{dc,BPCi} = m_G : m_{DG1} : \cdots : m_{DG,j} : \frac{3V^* V_{ac,bus} \cdot m}{2X_{v,1}} : \cdots : \frac{3V^* V_{ac,bus} \cdot m}{2X_{v,i}}, \quad (19)$$

where $\Delta P_{dc,G}$, $\Delta P_{dc,DGj}$ and$\Delta P_{dc,BPCi}$ are the power fluctuation of dc grid, dc voltage source DG_j and BPC_i, respectively.

When sharing the dc subgrid's power, the ac subgrid can be viewed as an ac voltage source. The power of BPCs comes from ac subgrid. Hence, the power sharing of BPCs should be proportional to the ac subgrid's capacity, which can be expressed as,

$$\frac{\sum_{i=1}^{M} \Delta P_{dc,BPCi}}{\Delta P_{dc,pcc} + \sum_{j=1}^{N} \Delta P_{dc,DGj}} = \frac{C_{AC}}{C_{DC}}. \quad (20)$$

Combining (13), (19), (20), the inverse droop coefficient m of $\theta - v_{dc}$ droop can be designed as,

$$m = \left(\frac{3V^{*2}}{2X_{AC}}\right)^{-1} \cdot \left(\frac{C_{AC}}{C_{DC}}\right)^2 \cdot m_{DC}, \quad (21)$$

where $m_{DC} = m_G + \sum_{j=1}^{N} m_{DGj}$ is the equivalent droop coefficient for the dc subgrid.

By adopting the $\theta - v_{dc}$ inverse droop control in (15), the BPCs can form the dc voltage whenever the dc grid voltage is lost. The dc load fluctuation can also be shared by the ac subgrid via BPCs, and the sharing radio is proportional to subgrids' capacities with the designed inverse droop coefficient in (21). Besides, by only controlling the dynamic phase angle, there is no frequency deviation in the steady state with the proposed control.

With the proposed ac and dc voltages supporting control strategies, the BPCs can support the voltage for the subgrid whose main grid is lost. Once there is an unintentional islanding, the BPCs can form the voltage for the subgrid, and enable the seamless mode switching. In addition, by adopting the designed virtual impedance and inverse droop coefficient, the power can be properly shared among BPCs according to BPCs' capacities. Furthermore, when there is a power fluctuation in one subgrid, the other subgrid can rapidly share the fluctuation in a coordinated manner, thus reducing the pressure on one single subgrid. The sharing ratio is designed as the ratio of ac and dc subgrids' capacities. The power sharing and power fluctuation sharing is illustrated in Fig. 5.

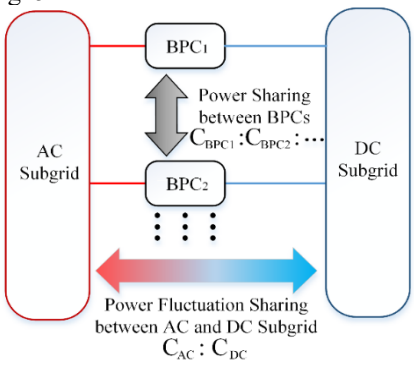

Fig. 5. The power sharing between BPCs and power fluctuation sharing between subgrids in the hybrid ac/dc microgrid

C. Implementation of Bidirectional Voltage Supporting Control during Mode Switching

The implementation of the proposed bidirectional voltage supporting controller is shown in Fig. 6. The control topology is decentralized, and only local information is used for the voltage support.

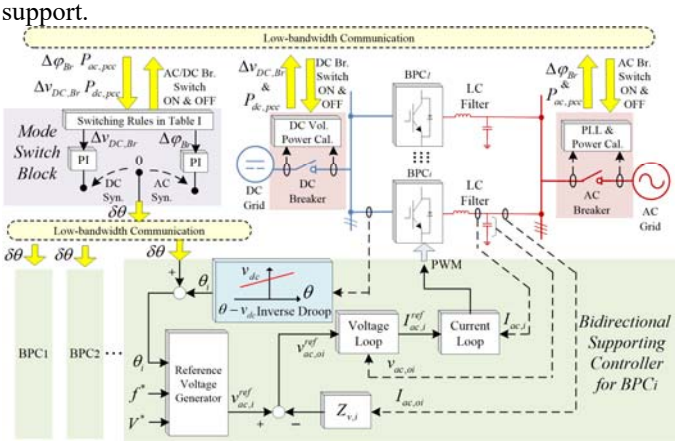

Fig. 6. The proposed bidirectional supporting controller implement with the mode switch

To realize the flexible mode switching in Section II, an additional mode switching block is designed. Through low-bandwidth communication, the voltage deviation $\Delta v_{dc,Br}$ and power $P_{dc,pcc}$ of the dc breaker, the phase angle deviation $\Delta \varphi_{Br}$ and power $P_{ac,pcc}$ of ac breaker are obtained by the mode switching block. According to the switch rules in Table I, the switch on/off decision is made and transferred to the corresponding ac and dc breakers. If the decision leads to closing a switch, synchronization is necessary. For the ac synchronization, the ac breaker phase angle difference $\Delta \varphi_{Br}$ is firstly fed to a PI controller, and its output $\delta\theta$ is transmitted to each BPC via low-bandwidth communication, and finally added to the BPCs' reference phase angle. For the dc side, the voltage difference between the two buses will lead to a severe power fluctuation due to low line resistance. Before the dc breaker switches on, dc synchronization is necessary to alleviate the voltage difference.

The voltage difference $\Delta v_{dc,Br}$ is also fed to a PI controller, and its output $\delta\theta$ is added to every BPC's reference phase angle. By adjusting the BPCs' phase angle, the power transferred into the dc subgrid is changed, in order to approach the dc grid's voltage. The ac and dc synchronizations are expressed as,

$$\text{AC synchronization: } \delta\theta = (k_{p,ac} + k_{i,ac}/\text{s}) \cdot \Delta\varphi_{Br}, \quad (22)$$

$$\text{DC synchronization: } \delta\theta = (k_{p,dc} + k_{i,dc}/\text{s}) \cdot \Delta v_{DC,Br}, \quad (23)$$

where $k_{p,ac}$, $k_{i,ac}$, $k_{p,dc}$ and $k_{i,dc}$ are the parameters of PI controller in the ac and dc synchronizations, respectively.

When there is an unintentional ac or dc islanding in the AC/DC GC mode, the operation mode of hybrid ac/dc microgrid will switch into the AC-GC DC-IS mode or AC-IS DC-GC mode. In these two switching modes, the BPCs can support the islanded subgrid with the proposed bidirectional voltage supporting control, while the interconnected subgrid is supported by the upper grid. As such, the additional voltage source is not required without decreasing the reliability of the system.

In the AC-GC DC-IS mode and AC-IS DC-GC mode, there is only one grid supporting the hybrid microgrid. In case of failure of this grid, one additional voltage source is adopted to provide backup power. In the AC/DC IS mode, the hybrid ac/dc microgrid operates in a totally islanding situation. The voltage source supports the voltage of one subgrid, and the BPCs can support the voltage of the other subgrid.

With the minimum reliance on additional voltage sources, the proposed control can support the ac and dc voltages for the hybrid microgrid in different modes, and enable the flexible seamless mode switching between multi modes.

IV. Stability Analysis of Hybrid AC/DC Microgrid

In this section, the stability of the hybrid ac/dc microgrid with the proposed control is analyzed in different modes. The ac and dc loads are characterized by the impedances $R_{ac,load} + jX_{ac,load}$ and $\text{R}_{dc,load}$. The renewable DGs operate in the maximum power point tracking (MPPT) mode, and their total power output is assumed to be constant in the dynamic process, which are $P_{ac,c}/Q_{ac,c}$ and $P_{dc,c}$. Section XIII (Appendix) shows the specific matrix definition of this section.

A. Hybrid AC/DC Microgrid Model in the AC/DC-GC Mode

In the dc subgrid, considering the power balance, we have

$$P_{dc,pcc} + \sum_{j=1}^{N} P_{dc,DGj} + \sum_{i=1}^{M} P_{dc,BPCi} + P_{dc,c} = \frac{v_{dc,bus}^2}{R_{dc,load}}. \quad (24)$$

For the BPC_i, the dc line resistance is $R_{dc,i}$, and the $P_{dc,BPCi}$ can be expressed as

$$P_{dc,BPCi} = \frac{(v_{dc,i} - v_{dc,bus})v_{dc,bus}}{R_{dc,i}}. \quad (25)$$

Linearizing and combining the (17), (18), (24), (25), we get

$$\boldsymbol{\Delta V_{dc}} = \boldsymbol{A} \cdot \boldsymbol{\Delta P_{dc,BPC}}, \quad (26)$$

where $\boldsymbol{\Delta V_{dc}} = [\Delta v_{dc,1} \ \cdots \ \Delta v_{dc,i} \ \cdots]^T$, $\boldsymbol{\Delta P_{dc,BPC}} = [\Delta P_{dc,BPC1} \ \cdots \ \Delta P_{dc,BPCi} \ \cdots]^T$.

In the proposed control, the dc voltage of BPC_i is filtered by a low-pass filter whose cutoff frequencies is ω_{vdc}. By linearizing (15), we have,

$$\Delta\theta_i = m \cdot \frac{\omega_{vdc}}{s + \omega_{vdc}} \cdot \Delta v_{dc,i}, \quad (27)$$

Combining (26), (27), we have,

$$\dot{\boldsymbol{X}} = -\omega_{vdc}\boldsymbol{X} + m\omega_{vdc} \cdot \boldsymbol{A} \cdot \boldsymbol{\Delta P_{dc,BPC}}, \quad (28)$$

where $\boldsymbol{X} = [\Delta\theta_1 \ \cdots \ \Delta\theta_i \ \cdots]^T$.

In the ac subgrid, the power balance is expressed by,

$$P_{ac,pcc} + \sum_{j=1}^{N} P_{ac,DGj} + \sum_{i=1}^{M} P_{ac,BPCi} + P_{ac,c} = \frac{3/2 \cdot R_{ac,load} \cdot V_{ac,bus}^2}{{R_{ac,load}}^2 + {X_{ac,load}}^2}, \quad (29)$$

$$Q_{ac,pcc} + \sum_{j=1}^{N} Q_{ac,DGj} + \sum_{i=1}^{M} Q_{ac,BPCi} + Q_{ac,c} = \frac{3/2 \cdot X_{ac,load} \cdot V_{ac,bus}^2}{{R_{ac,load}}^2 + {X_{ac,load}}^2}. \quad (30)$$

Linearizing and combining (2), (3), (6), (7)-(9), (29) and (30), and neglecting power losses in the BPC, and considering that $\Delta P_{ac,BPC}$ is the inverse to $\Delta P_{dc,BPC}$, we obtain

$$\Delta V_{ac,bus} = \frac{c_1 \cdot \boldsymbol{D_2} - c_2 \cdot \boldsymbol{D_1}}{b_1 c_2 - b_2 c_1} \boldsymbol{X}, \ \Delta\theta_o = \frac{b_1 \cdot \boldsymbol{D_2} - b_2 \cdot \boldsymbol{D_1}}{b_2 c_1 - b_1 c_2} \boldsymbol{X}, \quad (31)$$

$$\boldsymbol{\Delta P_{dc,BPC}} = -\boldsymbol{\Delta P_{ac,BPC}} = -\left(-\boldsymbol{D_2^T} \cdot \boldsymbol{E} + \boldsymbol{D_1^T} \cdot \boldsymbol{F} + \boldsymbol{G}\right)\boldsymbol{X}, \quad (32)$$

Combining (28), (32), the small signal model of the hybrid ac/dc microgrid in the AC/DC-GC mode is obtained as

$$\dot{\boldsymbol{X}} = (m\omega_{vdc} \cdot \boldsymbol{A} - \boldsymbol{W_{vdc}} + \boldsymbol{D_2^T} \cdot \boldsymbol{E} - \boldsymbol{D_1^T} \cdot \boldsymbol{F} - \boldsymbol{G}) \cdot \boldsymbol{X}. \quad (33)$$

B. Hybrid AC/DC Microgrid Model in other three Modes

In the AC-IS DC-GC mode, the ac grid is isolated from the hybrid microgrid. The $P_{ac,pcc}$ and $Q_{ac,pcc}$ is 0 in (29), (30). The factors b_1, c_1, b_2, c_2 in (31) are changed correspondingly, and the $\boldsymbol{E}$ and $\boldsymbol{F}$ are modified to refresh the hybrid microgrid model in (33).

In the AC-DC DC-IS mode, the dc grid is disconnected from the hybrid microgrid. The $P_{dc,pcc}$ is 0 in (24), which refreshes the $\boldsymbol{A}$ of the hybrid microgrid model in (33).

In the AC/DC IS mode, the $\boldsymbol{E}$ and $\boldsymbol{F}$ are the same as the AC-IS DC-GC mode, and $\boldsymbol{A}$ is the same as the AC-DC DC-IS mode. With the updated $\boldsymbol{A}$, $\boldsymbol{E}$ and $\boldsymbol{F}$ in (33), the hybrid microgrid model is obtained in the AC/DC IS mode.

C. Stability Analysis of Multi-Mode Hybrid AC/DC Microgrid

The stability of the hybrid ac/dc microgrid with the proposed control can be analyzed through the locus of the eigenvalues of $(m\omega_{vdc} \cdot \boldsymbol{A} - \boldsymbol{W_{vdc}} + \boldsymbol{D_2^T} \cdot \boldsymbol{E} - \boldsymbol{D_1^T} \cdot \boldsymbol{F} - \boldsymbol{G})$ in (33). For a typical hybrid ac/dc microgrid in Fig. 8(b) whose parameters are shown in Table. 2, the dominant eigenvalues with different $\theta - v_{dc}$ inverse droop coefficient m are shown in Fig. 7. m increases from 0 to $0.3V^{-1}$, which results in a stronger dc voltage feedback to the ac phase angle. In Fig. 7 (a), (b), the dominant poles move opposite to the imaginary axis, which means that the stability increases in the AC/DC GC and AC-GC DC-IS modes with increasing m. In Fig. 7(c), (d), the dominant poles move opposite to the imaginary axis, then move toward the imaginary axis. The stability of the hybrid microgrid firstly increases and then decreases in the AC-IS DC-GC and AC/DC IS modes.

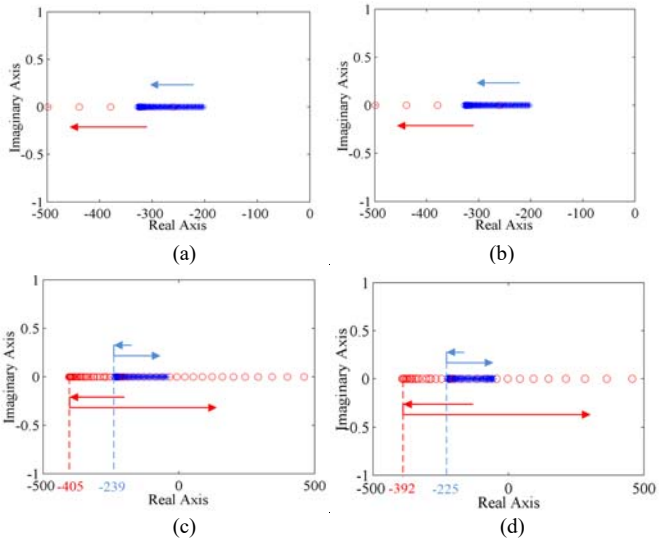

Fig. 7. Stability analysis of the hybrid ac/dc microgrid in different modes. (a) the AC/DC GC mode, (b) the AC-GC DC-IS mode, (c) the AC-IS DC-GC mode, (d) the AC/DC IS mode with a voltage source in the dc subgrid.

The above analysis shows that the stablity is more sensitive in the ac islanded mode than in the ac grid-connected mode with the proposed control. Besides, a smaller m can ensure the system stability, however, the dc voltage deviation will increase, when supporting the dc voltage according to (16).

V. Hardware-in-Loop Tests

To verify the effects of the proposed control, the HIL tests were conducted using the RT-LAB and STM32F407MCUs as shown in Fig. 8 (a). The test hybrid ac/dc microgrid is shown in Fig. 8 (b). It contains two BPCs, renewable DGs like PV and WT in ac and dc subgrids. The parameters of the hybrid microgrid are listed in Table II. The virtual impedance and inverse droop coefficient are designed as 1.2mH and 0.0146 V^{-1} according to (13) and (21).

TABLE II
PARAMETERS OF THE HYBRID MICROGRID

Microgrid Parameters	Rated Values
AC bus voltage (V^*/f^*)	311V/50Hz
DC bus voltage (v_{dc}^*)	600V
ac subgrid capacity (C_{AC})	150kW
dc subgrid capacity (C_{DC})	100kW
BPC1 capacity (C_{BPC1})	75kW
BPC2 capacity (C_{BPC2})	75kW
ac WT power output	60kW/20kVar
dc PV power output	40kW
ac grid impedance(Z_G)	10 m Ω/0.4mH
BPC1 ac line impedance ($Z_{ac,1}$)	20m Ω/0.06mH
BPC1 dc line impedance ($R_{dc,1}$)	6m Ω
BPC2 ac line impedance ($Z_{ac,2}$)	30m Ω/0.08mH
BPC2 dc line impedance ($R_{dc,2}$)	4m Ω
dc transformer droop coefficient (m_G)	7.5kW/V

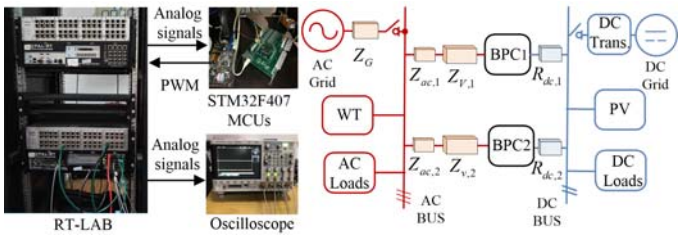

(a) (b)

Fig. 8. HIL tests setup: (a) HIL test facilities, (b) tested hybrid ac/dc microgrid.

A. Power Sharing test

Fig. 9 shows the dynamics of the hybrid ac/dc microgrid when the ac and dc load changes in the AC/DC-GC mode. In State I, the ac load is 105 kW, and the dc load is 40 kW. The dc load increases to 70 kW in State II. Then the dc load increases to the full load at 100 kW in State III. Finally, in State IV, a 45 kW/20 kvar ac load is added at the ac side.

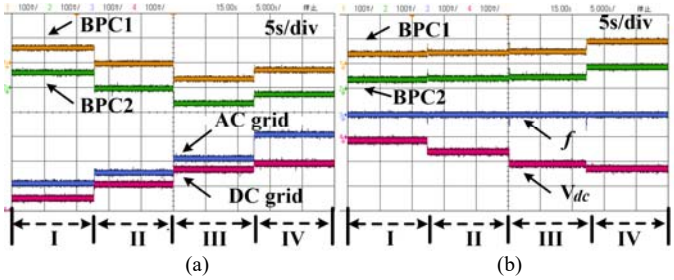

(a) (b)

Fig. 9. Dynamics of the hybrid ac/dc microgrid when ac and dc load changes. (a) Active power output of BPC1, BPC2, ac grid, dc grid (30kW/div). (b) Reactive power output of BPC1, BPC2 (30kvar/div) and dynamics of frequency (0.1Hz/div), dc voltage (5V/div).

Fig. 9(a) shows the active power output of BPC1, BPC2, ac grid and dc grid, respectively. For the BPCs, the power flowing from the dc subgrid to ac subgrid is considered as positive. When the dc load increases in States II and III, the active power output of BPC1 and BPC2 is reduced to feed the dc load. When the ac load increases in State IV, the BPCs' power increases to feed the ac load. The power sharing between BPC1 and BPC2 maintains the 1:1 ratio. The power output of ac grid and dc grid is increased synchronously when the ac and dc load increases, and the power radio is about 3:2. Fig. 9(b) shows the reactive power output of BPC1, BPC2 and frequency, dc voltage. The reactive power output sharing is maintained at 1:1 in the dynamic process. The ac and dc voltages are supported by the ac and dc grids in the AC/DC-GC mode. The frequency remains at 50 Hz, and the dc voltage drops by 6 V in the dc full load condition.

The above tests demonstrate that, with the proposed control, the active and reactive power of BPCs can be coordinated according to their capacities. Besides, the ac subgrid and dc subgrid can coordinate with each other to share the power fluctuation according to subgrids' capacities.

B. Ac Voltage Supporting Test

Fig. 10 shows the variations of power output of BPC1 and BPC2, frequency, phase angle deviation and ac voltage when the ac grid disconnects and reconnects with the hybrid ac/dc microgrid. In State I, the hybrid microgrid operates in the AC/DC-GC mode. To simulate the unintentional ac islanding, the ac breaker switches off in State II, and the operation mode is changed to the AC-IS DC-GC mode. In State III, the ac load increases by 45 kW/20 kvar to its full load. In State IV, the ac synchronization is implemented. In State V, the ac grid is reconnected to the hybrid microgrid after synchronization. The zoomed in switching dynamic scope is attached.

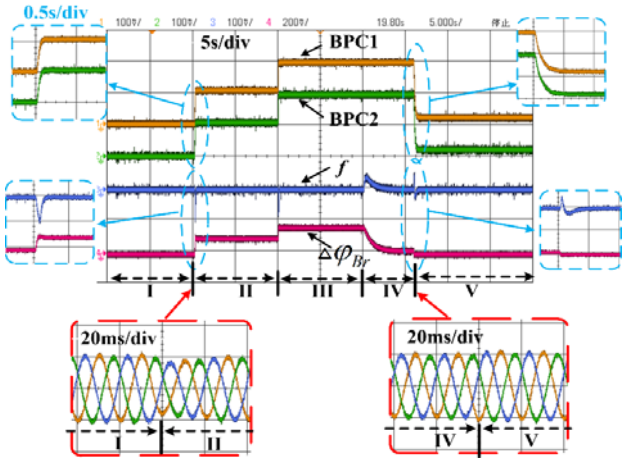

Fig. 10. Dynamics of power output of BPC1, BPC2(30kW/div), frequency (0.1Hz/div), phase angle deviation (0.2rad/div) and ac voltage (300V/div) when ac grid breaks and reconnects with hybrid ac/dc microgrid.

When an unintentional ac islanding occurs in State II, the power output of BPCs is adjusted to compensate the loss of the ac grid. From the zoomed in scope, there is a 0.1 Hz frequency drop lasting for 0.15 s during the dynamic process, and there is no frequency deviation in the steady state. The three-phase ac voltage is well supported by BPCs and voltage distortion is acceptable in the unintentional islanding process. In State III, the ac load increase is proportionally shared by BPCs with the radio of 1:1. In State IV, with the ac synchronization, the phase angle deviation is reduced to almost 0. In State V, there is a 0.05 Hz frequency fluctuation in the reconnection dynamic process after synchronization.

C. Dc Voltage Supporting Test

Fig. 11 shows the dynamics of power outputs of BPC1 and BPC2, dc grid voltage and dc subgrid voltage when the dc grid disconnects and reconnects with the hybrid ac/dc microgrid. In

State I, the hybrid microgrid operates in the AC/DC-GC mode. To simulate the unintentional dc islanding, the dc breaker switches off in State II, and the operation mode is changed to the AC-GC DC-IS mode. In State III, the dc load increases by 30 kW to its full load. In State IV, the dc synchronization is implemented. In State V, the dc grid is reconnected to the hybrid microgrid after the dc synchronization. The zoomed in switch dynamic scope is attached.

When an unintentional dc islanding happens in State II, the BPCs' power injected into the ac subgrid drops rapidly to share the dc load. From the zoomed in scope, it takes 0.5 s before the dc subgrid voltage stabilizes, and the amplitude of dc voltage oscillation is 8 V in the islanding dynamic state. In State III, the dc load increase is proportionally shared by BPCs with the radio of 1:1. With the support of BPCs, the dc voltage drop is 15 V (2.5% of reference voltage 600 V) in the dc full load condition. In State IV, the dc subgrid voltage approaches the dc grid voltage. In State V, the dc breaker switches on. With the support of the dc grid and BPCs, the dc voltage drop is alleviated by 5 V in the AC/DC-GC mode.

This test shows the BPCs can support the dc voltage when there is an unintentional dc islanding. In the dc islanded mode, the dc voltage drop is relatively higher with a 2.5% deviation. Power sharing among BPCs is proportional to their capacities.

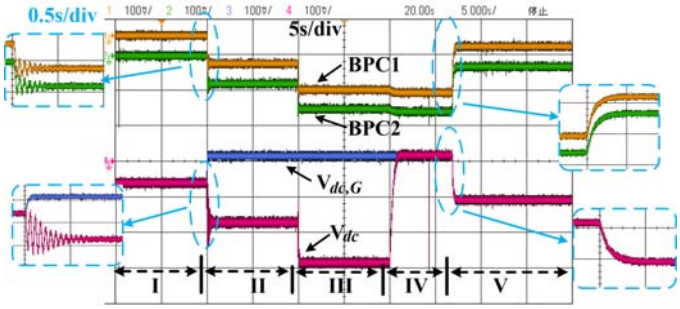

Fig. 11. Dynamics of power output of BPC1, BPC2(30kW/div), dc grid voltage, dc subgrid voltage (5V/div) when dc grid disconnects and reconnects with hybrid ac/dc microgrid.

VI. Conclusion

In this paper, a decentralized bidirectional voltage supporting control is proposed for the multi-mode hybrid ac/dc microgrid. By adopting the proposed control, the BPCs can support ac and dc voltages bidirectionally when there is an ac or dc islanding event, which enhances the reliability of the system without additional voltage sources. Besides, the ac and dc subgrids can share the power fluctuation together through BPCs. The proposed control also enables seamless mode switching between multi modes with corresponding mode switching rules. The system stability with the proposed control is analyzed in each mode. The real-time HIL test results show that the proposed control is effective for bidirectional voltage support and power sharing.

VII. References

[1] N. Hatziargyriou, "Microgrids: Architectures and Control", Wiley-IEEE Press, Year: 2014.

[2] D. E. Olivares et al., "Trends in microgrid control", *IEEE Trans. Smart Grid*, vol. 5, no. 4, pp. 1905-1919, Jul. 2014.

[3] D. Chen and L. Xu, "Autonomous DC voltage control of a DC microgrid with multiple slack terminals", *IEEE Trans. Power Syst.*, vol. 27, pp. 1897-1905, 2012.

[4] X. Liu, P. Wang and P. C. Loh, "A Hybrid AC/DC Microgrid and Its Coordination Control", *IEEE Trans. Smart Grid*, vol. 2, no. 2, pp. 278-286, June 2011.

[5] P. Wang, L. Goel, X. Liu and F. H. Choo, "Harmonizing ac and dc: A hybrid ac/dc future grid solution", *IEEE Power Energy Mag.*, vol. 11, no. 3, pp. 76-83, May 2013.

[6] N. Eghtedarpour and E. Farjah, "Power Control and Management in a Hybrid AC/DC Microgrid," *IEEE Trans. Smart Grid*, vol. 5, no. 3, pp. 1494-1505, May 2014.

[7] S. Inoue and H. Akagi, "A bidirectional isolated DC-DC converter as a core circuit of the next-generation medium-voltage power conversion system", *IEEE Trans. Power Electron.*, vol. 22, no. 2, pp. 535-542, Mar. 2007.

[8] B. S. H. Chew, Y. Xu and Q. Wu, "Voltage balancing for bipolar DC distribution grids: a power flow based binary integer multi-objective optimization approach", *IEEE Trans. Power Syst.*, vol. 34, no. 1, pp. 28-39, Jan. 2019.

[9] S. Cui, N. Soltau and R. W. D. Doncker, "A high step-up ratio soft-switching dc-dc converter for interconnection of MVDC and HVDC grids", *IEEE Trans. Smart Grid*, vol. 33, no. 4, pp. 2986-3001, Apr. 2018.

[10] N. Liu, C. Diduch, L. Chang and J. Su, "A reference impedance-based passive islanding detection method for inverter-based distributed generation system", *IEEE J. Emerg. Sel. Topics Power Electron.*, vol. 3, no. 4, pp. 1205-1217, Dec. 2015.

[11] P. Gupta, R. S. Bhatia and D. K. Jain, "Average absolute frequency deviation value based active islanding detection technique", *IEEE Trans. Smart Grid*, vol. 6, no. 1, pp. 26-35, Jan. 2015.

[12] A. Khamis, Y. Xu, Z. Y. Dong and R. Zhang, "Faster detection of microgrid islanding events using an adaptive ensemble classifier", *IEEE Trans. Smart Grid*, vol. 9, no. 3, pp. 1889-1899, May 2018.

[13] C. N. Papadimitriou, V. A. Kleftakis, N. D. Hatziargyriou, "A novel method for islanding detection in DC networks", *IEEE Trans. Sustain. Energy*, vol. 8, no. 1, pp. 441-448, Jan. 2017.

[14] N. Pogaku, M. Prodanovic, T. C. Green, W. L. Kling and L. Van Der Sluis, "Modeling analysis and testing of autonomous operation of an inverter-based microgrid", *IEEE Trans. Power Electron.*, vol. 22, no. 2, pp. 613-625, Mar. 2007.

[15] Y. Sun et al., "An f-P/Q droop control in cascaded-type microgrid", *IEEE Trans. Power Syst.*, vol. 33, no. 1, pp. 1136-1138, Jan. 2018.

[16] H. Xin, R. Zhao, L. Zhang, Z. Wang, K. P. Wong and W. Wei, "A decentralized hierarchical control structure and self-optimizing control strategy for F-P Type DGs in islanded microgrids," *IEEE Trans. Smart Grid*, vol. 7, no. 1, pp. 3-5, Jan. 2016.

[17] J. C. Vasquez, J. M. Guerrero, A. Luna, P. Rodriguez and R. Teodorescu, "Adaptive droop control applied to voltage-source inverters operating in grid-connected and islanded modes", *IEEE Trans. Ind. Electron.*, vol. 56, no. 10, pp. 4088-4096, Oct. 2009.

[18] J. He and Y. W. Li, "An enhanced microgrid load demand sharing strategy," *IEEE Trans. Power Electron.*, vol. 27, no. 9, pp. 3984-3995, Sept. 2012.

[19] Y. W. Li and C. Kao, "An accurate power control strategy for power-electronics-interfaced distributed generation units operating in a low-voltage multibus microgrid", *IEEE Trans. Power Electron.*, vol. 24, no. 12, pp. 2977-2988, Dec. 2009.

[20] Z. Wang, B. Chen, J. Wang, M. M. Begovic and C. Chen, "Coordinated energy management of networked microgrids in distribution systems", *IEEE Trans. Smart Grid*, vol. 6, no. 1, pp. 45-53, Jan. 2015.

[21] B. Zakeri and S. Syri, "Electrical energy storage systems: A comparative life cycle cost analysis", *Renewable and Sustainable Energy Reviews*, vol. 42, pp. 569-596, Jan. 2016.

[22] B. Zhao, X. Zhang, J. Chen, C. Wang and L. Guo, "Operation optimization of standalone microgrids considering lifetime characteristics of battery energy storage system", *IEEE Trans. Sustain. Energy*, vol. 4, no. 4, pp. 934-943, Oct. 2013.

[23] Y. Xia, Y. Peng, P. Yang, M. Yu and W. Wei, "Distributed coordination control for multiple bidirectional power converters in a hybrid AC/DC microgrid", *IEEE Trans. Power Electron.*, vol. 32, no.6, pp. 4949 – 4959, Jun. 2017.

[24] P. Yang, Y. Xia, M. Yu, W. Wei and Y. Peng, "A decentralized coordination control method for parallel bidirectional power converters in a hybrid AC/DC microgrid", *IEEE Trans. Ind. Electron.*, vol. 65, no. 8, pp. 6217-6228, Aug. 2018.

[25] X. Li *et al.*, "A unified control for the DC-AC interlinking converters in hybrid AC/DC microgrids", *IEEE Trans. Smart Grid*, vol. 9, no. 6, pp. 6540-6553, Nov. 2018.

[26] J. Wang, C. Jin and P. Wang, "A uniform control strategy for the interlinking converter in hierarchical controlled hybrid AC/DC microgrids", *IEEE Trans. Ind. Electron.*, vol. 65, no. 8, pp. 6188-6197, Aug. 2018.

[27] F. Chen, W. Zhang, R. Burgos and D. Boroyevich, "Droop voltage range design in DC micro-grids considering cable resistance", *Proc. IEEE Energy Convers. Congr. Expo.*, pp. 770-777, 2014.